C SAFOD supplements

C.1   Reading the raw data

240 channels of data were recorded with a Geometrics Geode recording system.
The digital data were passed to a workstation where records of 16 s length were
scanned for event detection. Whenever events were detected the record was stored
to disk in seg2 format (format details are given in Pullan, 1990). The following
MatLab script was used to read the raw data.

```
function [data,N,NS,dt,trhead]=readseg2(filename)
%%%%% Program to read seg2 data
%%%%% based on Geophysics paper of S.E. Pullan, 1990

fid = fopen(filename,'r')

id = fread(fid,1,'int16=>int16'); % Bytes 0 & 1  low / big endian test
rev = fread(fid,1,'int16=>int16'); % Bytes 2 & 3  revision number
M = fread(fid,1,'short=>short');   % Bytes 4 & 5  size of trace pointers
N = fread(fid,1,'int16=>int16')    % Bytes 6 & 7  number of traces
strtermsize1 = fread(fid,1,'uint8=>int8');
strtermchar1 = fread(fid,1,'char=>char');
strtermsize2 = fread(fid,1,'uint8=>int8');
strtermchar2 = fread(fid,1,'char=>char');
lntermsize1 = fread(fid,1,'uint8=>int8');
lntermchar1 = fread(fid,1,'char=>char');

fseek(fid,32,'bof');     %%% put pointer to the trace pointer subblock

for i=1:M/4
   trpointer(i) = fread(fid,1,'uint32=>uint32'); %%% pointer to trace descriptor block
end

i=1;
    %%% put pointer to the sample number given in the first trace descriptor block
    fseek(fid,double(trpointer(i)+8),'bof');
    %%% Bytes 8,9,10 & 11 number of samples in the first data block
    NS = fread(fid,1,'int32=>int32')
    %%% assign an array of the size of the expected data
    data=zeros(NS,N);

 while (trpointer(i) ~= 0)
    %%% put pointer to the start of the trace descriptor block
    fseek(fid,double(trpointer(i)),'bof');
    %%% Bytes 0 & 1 Trace descriptor ID
```

```
    trid = fread(fid,1,'int16=>int16');
    %%% Bytes 2 & 3 Size of the  trace descriptor block
    X = fread(fid,1,'int16=>int16');
    %%% Bytes 4,5,6 & 7  Size of the corresponding data block
    Y = fread(fid,1,'int32=>int32');
    %%% Bytes 8,9,10 & 11  Number of samples
    NS = fread(fid,1,'int32=>int32');
    %%% Bytes 12  Data Format Code (1=='int16', 2=='int32';
    DFC= fread(fid,1,'uint8=>uint8');
    %%%     3=='20-bit float'; 4=='float32' and 5=='float64')
    %disp([num2str(i), '...' ,num2str(trid), '...' , num2str(DFC)] )


    %%% put pointer to the start of the trace header
    fseek(fid,double(trpointer(i)+33),'bof');
    %%% read trace header
    header=fread(fid,double(X-32),'char=>char');
    %%% find the entry for the sample interval
    k=findstr(header', 'SAMPLE_INTERVAL');
    %%% get sample interval (usually in s)
    dt=str2num(header(k+16:k+23)');
    % find the entry for the receiver location
    k=findstr(header', 'RECEIVER_LOCATION');
    %%% get the receiver location
    rloc(i)=str2num(header(k+17:k+23)');
    %%% store header entries to build a header structure later
    dummy(i,1) = cellstr(header');

    %%% put pointer to the start of the trace
    fseek(fid,double(trpointer(i))+double(X),'bof');
    %%% read data
    data(:,i) = fread(fid,double(NS),'float32');
    i=i+1;
 end

%%% write header info in a structure
trhead = cell2struct(dummy, 'header', double(N));

%%% access trhead(i).header
clear dummy;
```

Note that the raw data contained 241 channels. Channels 1-240 contained wave-forms and channel 241 was an auxiliary channel.

C.2   Electronic noise

When visually inspecting the extracted raw data (before rotating them into geo-graphical coordinates) some electronic noise pulses were recognized in some of the data files. Interestingly, the noise pulses occurred almost every 200 ms and had the same onset time in the data files (at about 11.55 s of the record, see Figure C.1). A zoom of this repeating noise is shown in Figure C.2.

The same onset time of this noise indicated that its occurrence was related to the recording system. The recording system consisted of ten 24 channel boxes and a recording box related problem would most likely show high correlation within the same box. For this reason a cross-correlation of the noise pulse over all channels
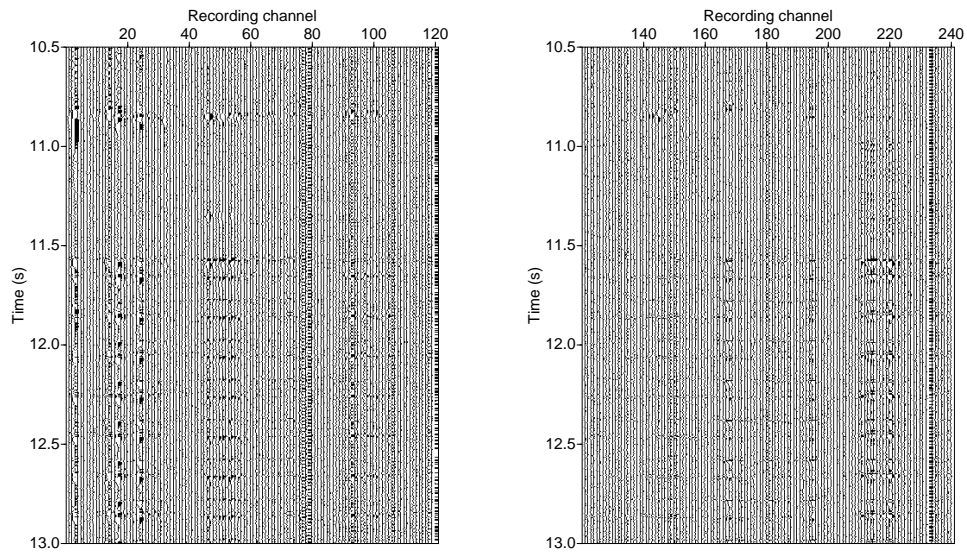
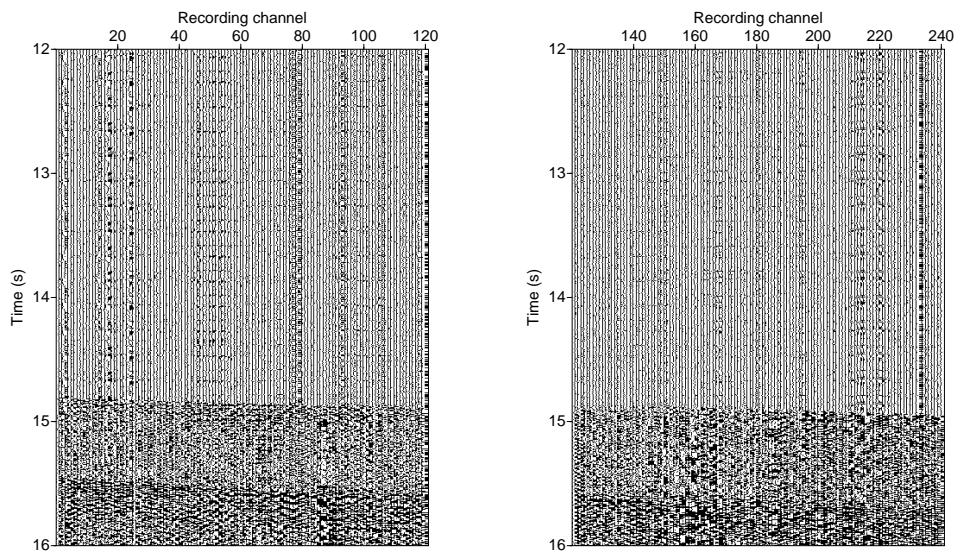Figure C.1: Electric noise contaminating the records from 11.55 s.

Figure C.2: Electric noise.

was performed. The result is shown in Figure C.3 where the red rectangles frame the channels recorded with the same 24 channel box. It can be clearly seen, that high correlation is encountered even outsite of the 24 channel boxes (e.g., at channels 211-223). This observation indicates that the noise is caused by some source outside the recording units. The actual reason is still under discussion.
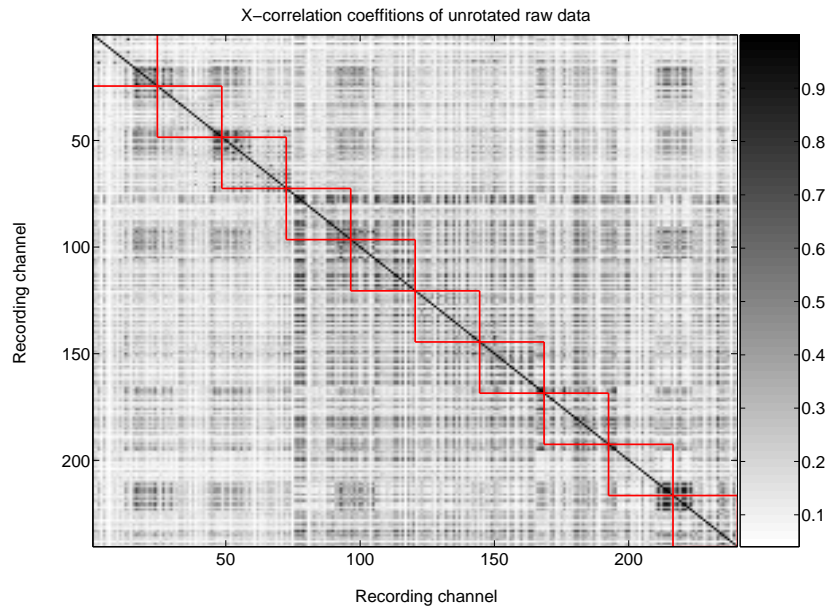

Figure C.3: Cross-correlation of the noise traces between 12-14 s.

Nevertheless, it is very intuitive that noise like this triggers the event detection independent of which algorithm is used. The noise spikes contained high intensities over the whole frequency bandwidth (the frequency analysis looked as if a delta pulse was analyzed). Hence filtering in the frequency domain did not provide a solution. Also linear predictive filters (as described in Jackson, 1989) were tested but these filters also changed the wavelet of the singal which destroys the signal polarization. The most promising results were obtained by building an averaged reference trace for each channel that did only contain the repeating noise pulse. Subtracting the reference noise traces from the data mostly removed the noise spikes.

C.3 Receiver orientation of the P/GSI array

PGS/I provided us with azimuth and dip information for each receiver component deployed at the third stage which was also the deepest deployment. The values are given in Table C.1 and C.2.

These given dips $\theta(tool, component)$ and azimuths $\phi(tool, component)$ were

used to build an eigenvector matrix for each tool in the following way:

$$\mathbf{B} = \begin{pmatrix} xn(tool) & xe(tool) & xv(tool) \\ yn(tool) & ye(tool) & yv(tool) \\ zn(tool) & ze(tool) & zv(tool) \end{pmatrix} \tag{C.1}$$

with

$$
\begin{aligned}
xn(tool) &= \cos(\theta(tool, 2)) \cdot \cos(\phi(tool, 2)) \\
yn(tool) &= \cos(\theta(tool, 2)) \cdot \sin(\phi(tool, 2)) \\
zn(tool) &= \sin(\theta(tool, 2)) \\
xe(tool) &= \cos(\theta(tool, 3)) \cdot \cos(\phi(tool, 3)) \\
ye(tool) &= \cos(\theta(tool, 3)) \cdot \sin(\phi(tool, 3)) \\
ze(tool) &= \sin(\theta(tool, 3)) \\
xv(tool) &= \cos(\theta(tool, 1) \cdot \cos(\phi(tool, 1)) \\
yv(tool) &= \cos(\theta(tool, 1)) \cdot \sin(\phi(tool, 1)) \\
zv(tool) &= \sin(\theta(tool, 1)).
\end{aligned}
\tag{C.2}
$$

The first column of B represents the (x,y,z)-coordinates of the x-axis in which the data are given relative to the geographical coordinate system and the second column represents the (x,y,z)-coordinates of the y-axis and the third represents the (x,y,z)-coordinates of the z-axis, respectively. The data U_2, U_3 and U_1 have been rotated into geographical coordinates with

$$
\begin{aligned}
u_n &= B(1,1) \cdot U_2 + B(1,2) \cdot U_3 + B(1,3) \cdot U_1 \\
u_e &= B(2,1) \cdot U_2 + B(2,2) \cdot U_3 + B(2,3) \cdot U_1 \\
u_v &= B(3,1) \cdot U_2 + B(3,2) \cdot U_3 + B(3,3) \cdot U_1.
\end{aligned}
\tag{C.3}
$$

For this documentation we use U_2, U_3 and U_1 to reflect the component notation in the raw data header file. Component 1 represents the component in-line with the borehole and the components 2 and 3 respresent the 'horizontal' components where component 3 is defined 90° clockwise from component 2. In geographical coordinates u_n points positive North, u_e positive East and u_z positive down.

C.3. Receiver orientation of the P/GSI array

Tool	Depth (m) bls	Compo-nent	Azimuth rel. to North	Dip (-90 vertically up)	Tool	Depth (m) bls	Compo-nent	Azimuth rel. to North	Dip (-90 vertically up)
1	877.79	1	217.48	-81.37	21	1153.58	1	207.47	-50.95
1	877.79	2	53.38	-8.30	21	1153.58	2	319.43	-16.88
1	877.79	3	143.04	2.33	21	1153.58	3	61.24	-33.99
2	892.82	1	214.76	-79.57	22	1165.25	1	208.25	-48.90
2	892.82	2	271.29	5.80	22	1165.25	2	105.65	-10.77
2	892.82	3	0.41	-8.64	22	1165.25	3	186.77	39.07
3	907.75	1	212.09	-77.65	23	1176.55	1	209.22	-46.75
3	907.75	2	296.25	1.28	23	1176.55	2	212.93	43.19
3	907.75	3	25.98	-12.28	23	1176.55	3	301.19	-1.86
4	922.59	1	210.23	-75.63	24	1187.45	1	210.37	-44.72
4	922.59	2	321.81	-5.38	24	1187.45	2	107.33	-12.83
4	922.59	3	53.08	-13.29	24	1187.45	3	185.31	42.45
5	937.28	1	208.95	-73.53	25	1197.99	1	211.32	-43.08
5	937.28	2	357.80	-14.20	25	1197.99	2	19.41	-46.30
5	937.28	3	89.89	-8.17	25	1197.99	3	115.70	-5.98
6	951.81	1	207.87	-71.36	26	1208.26	1	211.70	-41.95
6	951.81	2	263.45	10.80	26	1208.26	2	332.48	-29.65
6	951.81	3	350.52	-15.01	26	1208.26	3	84.81	-33.73
7	966.15	1	206.81	-69.26	27	1218.37	1	211.86	-41.49
7	966.15	2	100.21	-6.18	27	1218.37	2	318.59	-18.04
7	966.15	3	187.98	19.72	27	1218.37	3	66.27	-43.01
8	980.30	1	206.07	-67.80	28	1228.46	1	212.01	-41.43
8	980.30	2	293.86	0.90	28	1228.46	2	42.21	-48.11
8	980.30	3	23.50	-22.18	28	1228.46	3	126.52	5.08
9	994.37	1	206.04	-67.26	29	1238.54	1	212.18	-41.52
9	994.37	2	302.88	-2.86	29	1238.54	2	311.90	-10.8
9	994.37	3	34.07	-22.54	29	1238.54	3	53.47	-46.46
10	1008.41	1	206.29	-67.32	30	1248.66	1	212.35	-41.56
10	1008.41	2	223.35	21.78	30	1248.66	2	110.39	-13.16
10	1008.41	3	310.93	-6.03	30	1248.66	3	186.64	45.46
11	1022.49	1	206.64	-67.36	31	1258.76	1	212.72	-41.31
11	1022.49	2	45.85	-21.50	31	1258.76	2	7.38	-45.8
11	1022.49	3	133.17	6.77	31	1258.76	3	111.06	-12.95
12	1036.55	1	207.11	-66.89	32	1268.78	1	213.27	-40.74
12	1036.55	2	13.35	-22.51	32	1268.78	2	64.21	-44.88
12	1036.55	3	105.40	-4.95	32	1268.78	3	137.59	16.02
13	1050.52	1	207.68	-65.94	33	1278.65	1	213.84	-39.88
13	1050.52	2	231.86	22.16	33	1278.65	2	114.03	-11.53
13	1050.52	3	318.20	-8.9	33	1278.65	3	191.02	47.81
14	1064.38	1	208.23	-64.39	34	1288.32	1	214.57	-38.99
14	1064.38	2	19.62	-25.36	34	1288.32	2	115.58	-10.93
14	1064.38	3	111.21	-3.35	34	1288.32	3	192.78	48.92
15	1078.00	1	208.35	-62.17	35	1297.83	1	215.25	-38.37
15	1078.00	2	195.92	27.28	35	1297.83	2	275.28	32.25
15	1078.00	3	288.57	5.13	35	1297.83	3	339.00	-35.06
16	1091.32	1	208.02	-59.57	36	1307.24	1	215.58	-37.86
16	1091.32	2	22.51	-30.31	36	1307.24	2	169.03	41.49
16	1091.32	3	113.92	-2.4	36	1307.24	3	283.89	25.43
17	1104.28	1	207.59	-57.23	37	1316.54	1	215.78	-37.30
17	1104.28	2	261.37	20.82	37	1316.54	2	285.66	24.31
17	1104.28	3	341.58	-24.09	37	1316.54	3	350.84	-42.9
18	1116.95	1	207.16	-55.41	38	1325.71	1	216.00	-36.91
18	1116.95	2	331.27	-21.14	38	1325.71	2	294.86	14.43
18	1116.95	3	72.14	-26.00	38	1325.71	3	7.37	-49.45
19	1129.37	1	206.79	-53.96	39	1334.84	1	216.16	-36.88
19	1129.37	2	121.27	3.25	39	1334.84	2	166.23	40.63
19	1129.37	3	213.62	35.85	39	1334.84	3	282.98	27.68
20	1141.59	1	206.91	-52.62	40	1344.00	1	216.25	-36.85
20	1141.59	2	85.04	-21.97	40	1344.00	2	43.96	-52.90
20	1141.59	3	162.35	28.57	40	1344.00	3	129.04	3.71

Table C.1: Receiver orientations of the upper part of the P/GSI array deployed in the SAFOD Main Hole. Orientations are obtained from far-offset shots.

Tool	Depth (m) bls	Compo- nent	Azimuth rel. to North	Dip (-90 vertically up)	Tool	Depth (m) bls	Compo- nent	Azimuth rel. to North	Dip (-90 vertically up)
41	1353.12	1	216.43	-36.50	61	1531.94	1	216.44	-34.75
41	1353.12	2	24.69	-52.92	61	1531.94	2	300.82	8.03
41	1353.12	3	122.23	-5.66	61	1531.94	3	19.59	-54.06
42	1362.13	1	216.82	-36.06	62	1540.66	1	216.49	-35.43
42	1362.13	2	165.99	40.94	62	1540.66	2	333.56	-32.61
42	1362.13	3	283.78	28.26	62	1540.66	3	93.17	-37.67
43	1371.06	1	217.18	-35.82	63	1549.60	1	216.53	-35.92
43	1371.06	2	260.78	45.10	63	1549.60	2	31.70	-53.98
43	1371.06	3	325.24	-23.25	63	1549.60	3	124.86	-2.30
44	1379.97	1	217.40	-35.78	64	1558.54	1	216.58	-35.73
44	1379.97	2	282.08	30.69	64	1558.54	2	83.96	-43.27
44	1379.97	3	343.24	-39.10	64	1558.54	3	146.92	25.78
45	1388.88	1	217.58	-35.76	65	1567.40	1	216.57	-35.70
45	1388.88	2	332.71	-30.53	65	1567.40	2	10.94	-51.45
45	1388.88	3	91.52	-39.26	65	1567.40	3	117.29	-12.64
46	1397.78	1	217.74	-35.76	66	1576.33	1	216.32	-36.17
46	1397.78	2	138.44	14.46	66	1576.33	2	262.66	43.36
46	1397.78	3	246.70	50.55	66	1576.33	3	326.37	-25.13
47	1406.69	1	217.93	-35.85	67	1585.39	1	216.04	-36.38
47	1406.69	2	120.37	-10.32	67	1585.39	2	120.25	-7.80
47	1406.69	3	196.78	52.23	67	1585.39	3	199.96	52.52
48	1415.63	1	218.09	-36.02	68	1594.40	1	215.99	-36.12
48	1415.63	2	154.39	31.36	68	1594.40	2	59.90	-51.40
48	1415.63	3	273.10	38.25	68	1594.40	3	134.75	11.79
49	1424.62	1	218.24	-36.30	69	1603.36	1	216.10	-35.86
49	1424.62	2	112.98	-19.71	69	1603.36	2	158.40	36.47
49	1424.62	3	180.35	47.05	69	1603.36	3	277.61	33.43
50	1433.68	1	218.09	-36.40	70	1612.26	1	216.40	-35.84
50	1433.68	2	278.49	33.83	70	1612.26	2	263.31	43.40
50	1433.68	3	339.88	-35.54	70	1612.26	3	326.53	-25.47
51	1442.70	1	217.66	-36.07	71	1621.20	1	216.76	-36.15
51	1442.70	2	315.37	-10.43	71	1621.20	2	120.07	-9.06
51	1442.70	3	58.98	-51.97	71	1621.20	3	198.13	52.37
52	1451.63	1	217.35	-35.77	72	1630.24	1	217.01	-36.78
52	1451.63	2	47.32	-53.81	72	1630.24	2	280.52	30.82
52	1451.63	3	130.79	4.76	72	1630.24	3	342.74	-38.00
53	1460.52	1	217.33	-35.75	73	1639.46	1	217.11	-37.37
53	1460.52	2	230.33	53.54	73	1639.46	2	180.79	46.53
53	1460.52	3	311.84	-6.22	73	1639.46	3	291.96	18.90
54	1469.43	1	217.42	-35.93	74	1648.74	1	217.45	-37.70
54	1469.43	2	114.94	-16.61	74	1648.74	2	268.62	39.06
54	1469.43	3	184.68	49.26	74	1648.74	3	332.37	-28.60
55	1478.40	1	217.32	-36.21	75	1658.09	1	217.94	-37.61
55	1478.40	2	270.56	39.25	75	1658.09	2	55.01	-51.14
55	1478.40	3	332.37	-30.04	75	1658.09	3	134.46	8.39
56	1487.44	1	217.28	-36.56	76	1667.34	1	218.13	-36.83
56	1487.44	2	95.06	-35.72	76	1667.34	2	65.06	-49.97
56	1487.44	3	156.66	33.49	76	1667.34	3	138.48	13.48
57	1496.56	1	217.10	-36.62	77	1676.36	1	218.14	-36.03
57	1496.56	2	303.09	5.37	77	1676.36	2	257.14	46.90
57	1496.56	3	25.95	-52.86	77	1676.36	3	323.79	-20.35
58	1505.62	1	216.50	-36.12	78	1685.27	1	218.14	-35.67
58	1505.62	2	87.97	-40.48	78	1685.27	2	338.50	-35.15
58	1505.62	3	150.08	28.72	78	1685.27	3	98.00	-34.97
59	1514.53	1	216.17	-35.42	79	1694.14	1	218.32	-35.57
59	1514.53	2	14.74	-52.62	79	1694.14	2	357.73	-46.72
59	1514.53	3	118.66	-10.41	79	1694.14	3	112.15	-21.27
60	1523.29	1	216.28	-34.83	80	1703.00	1	218.53	-35.57
60	1523.29	2	300.53	8.19	80	1703.00	2	159.86	36.02
60	1523.29	3	19.13	-53.94	80	1703.00	3	279.46	34.19

Table C.2: Receiver orientations of the lower part of the P/GSI array deployed in the SAFOD Main Hole. Orientations are obtained from far-offset shots.

C.4 Velocity models

The velocity model provided to us by Cliff Thurber in 2006 contained the following model information. The coordinate origin is at the SAFOD Pilot Hole (35 58.455 N, 120 33.126 W) and sea level; +x points N-40-E and +y points N-130-E. It extended from x = -6000 m to x=10000 m, y = -8000 m to y = 8000 m and z = -500 m to 10000 m. It was decided to align the migration model to this velocity model orientation in order to avoid rotation induced gaps. The gridspacing of this provided velocity model is irregular as shown in Figure C.4. A linear 3D interpolation (with a standard MatLab function) to a regular grid of 100 m spacing was performed.
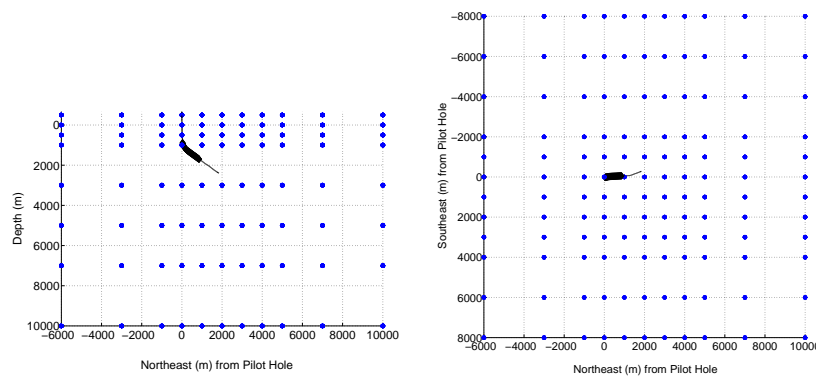
Figure C.4: Grid layout of the Thurber 2006 velocity model.

The velocity model called Thurber 2007 has the same orientation and extensions as the model provided in 2006. Model specifications only differed in the grid spacing around the SAFOD Pilot Hole /Main Hole respectively as shown in Figure C.5. Again a linear interpolation to a 100 m regular grid was performed.
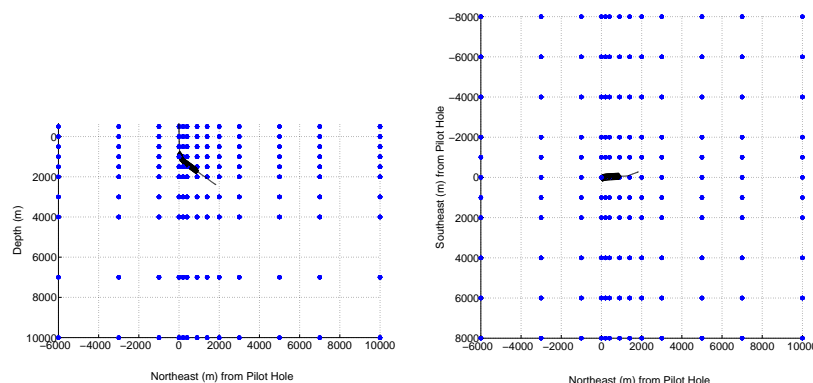
Figure C.5: Grid layout of the Thurber 2007 velocity model.

The velocity model provided by Haijiang Zhang in 2007 has the same orienta-

tion and the same origin as the models from C. Thurber. From x = -6000 m to x=10000 m, y = -8000 m to y = 8000 m and z = -500 m to 10000 m it has the same grid spacing as the Thurber 2007 model. It contains one more grid line on each edge, for x and y at -240000 m and 240000 m, for z at -150000 m and 340000 m. It is assumed that these gridpoints are only set to assign boundary conditions but do not provide useful information for the target of interest. Hence only the values between x = -6000 m to x=10000 m, y = -8000 m to y = 8000 m and z = -500 m to 10000 m were considered and interpolated to a regular grid of 100 m spacing.

The three velocity models provided by Steven Roecker had different axis orientation as well as different extensions compared with the models from C. Thurber and H. Zhang. They extended from x = -11000 m to x=10400 m, y = -13200 m to y = 11800 m and z = -1600 m to 15000 m. The x-axis was oriented 41.5° counterclockwise from East. The origin for these three models is located at UTM NAD83: Easting (m) 723397.49 and Northing (m) 3983459.12 (pers. comm. Steven Roecker, 2007). The orientation as well as the origin differs from those used in Roecker et al. (2004). S. Roecker provided the grid points in their local frame as well as in UTM NAD 27 and NAD83 coordinates. It was decided to keep the model setup for the migration in the coordinate system of C. Thurber. Therefore the Pilot Hole UTM NAD83 coordinates were subtracted from the NAD83 grid coordinates (see Figure C.6). Then the horizontal grid coordinates were rotated into the coordinate system used by Thurber and Zhang, where +x points N-40-E and +y points N-130-E. Finally we performed a 3D linear interpolation in order to obtain a velocity model with 100 m grid spacing extending from x = -6000 m to x=10000 m, from y = -8000 m to y = 8000 m and from z = -500 m to 10000 m. The new model is smaller than the original model provided by S. Roecker and hence we did not create data gaps during the rotation / transformation procedure.
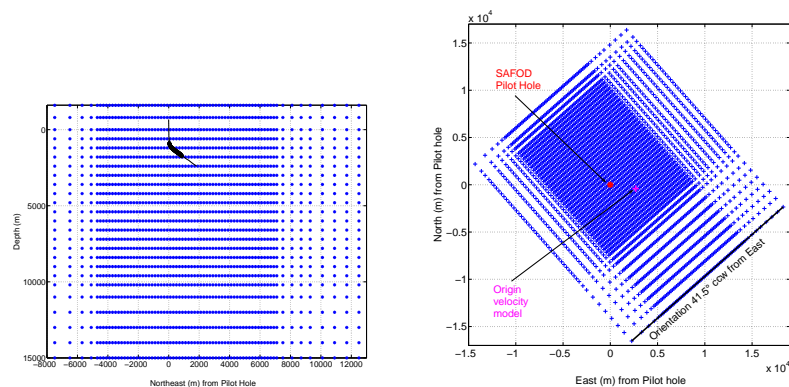

Figure C.6: Grid layout of the Roecker 2007 velocity models.